Extended Finite Element Method for Statics and Vibration Analyses on Cracked Bars and Beams

F. Mottaghian [1], A. Darvizeh [2], A. Alijani [2,*]

[1]*Department of Mechanical Engineering, University of Guilan, Rasht, Iran*
[2]*Department of Mechanical Engineering, Bandar Anzali Branch, Islamic Azad University, Bandar Anzali, Iran*

ABSTRACT

In this paper, the extended finite element method (XFEM) is employed to investigate the statics and vibration problems of cracked isotropic bars and beams. Three kinds of elements namely the standard, the blended and the enriched elements are utilized to discretize the structure and model cracks. Two techniques referred as the increase of the number of Gauss integration points and the rectangle sub-grid are applied to refine the integration within the blended and enriched elements of the beam in which the priority of the developed rectangle sub-grid technique is identified. The stiffness and the mass matrices of the beam are extended by considering the Heaviside and the crack tip functions. In a plane stress analysis, the effects of various crack positions and depths, different boundary conditions and other geometric parameters on the displacement and the stress contours are detected. Moreover, in a free vibration analysis, changes of the natural frequencies and the mode shapes due to the aforementioned effects are determined.   © 2018 IAU, Arak Branch. All rights reserved.

Keywords: Extended finite element method; Statics and vibration; Cracked bars and beams; Increasing Gauss integration points; Rectangle sub-grid.

1   INTRODUCTION

ENGINEERING structures such as buildings, highways, aircraft, etc. may be destroyed due to geometric and material discontinuities usually created during their manufacturing processes or the working life. The investigation of the mechanical phenomena in discontinuous structures requires a more detailed understanding of the fracture mechanics concepts. So, the mathematical modeling of the discontinuities especially the crack and the development of the numerical methods for solving these problems are regularly attended by many designers and researchers. The finite element method was fully discussed by Wriggers [1], Reddy [2] and Logan[3]. The vibration analysis of different structures can be found in Leissa [4], Rao [5] and Cook [6]. Kahya and Turan [7] employed a finite element model for vibration and buckling of functionally graded beams based on the first-order shear deformation. Darvizeh et al. [8] presented pre- and post-buckling behaviors of beams made of functionally graded materials using the finite element formulation based on the Euler-Bernoulli beam theory. Elasto-plastic pre- and post-buckling behaviors of FGMs beams were investigated with a continuum-based finite element method by Alijani

_____
[*]Corresponding author. Tel.: +98 134 440 0486.
E-mail address: alijani@iaubanz.ac.ir (A. Alijani).

et al. [9]. The different theoretical techniques such as the discrete spring model, the smeared crack model, the local and non-local models, fracture mechanic theories, the meshless method, XFEM and etc. are used for modeling strong and weak discontinuities in structures. The concepts of fracture mechanics and XFEM were introduced by Mohammadi [10]. Different applications in XFEM were discussed in [11]. Biondi and Caddemi [12] proposed closed-form solutions of Euler–Bernoulli beams with discontinuities which were modeled as singularities of the flexural stiffness via distribution theory. A simple method was employed to model a crack as an element on a beam with stepped cross sections in [13]. Skrinar formulated the finite element method of a beam with an arbitrary number of transverse cracks replaced by linear rotational springs [14] . Yang et al. studied the bending deformation of the Timoshenko beam with cracks in which the crack with a gap was represented by means of an equivalent nonlinear internal rotational spring [15]. Also, Moës and et al. presented a new technique for modeling crack in the finite element method in which a standard displacement was enriched near a crack by incorporating discontinuous through a partition of unity method [16]. Then, the extended finite element method was applied to model the growth of arbitrary cohesive cracks by Moës and Belytschko [17]. Also, Sukumar and et al. described an extended finite element method for three-dimensional crack modeling. A discontinuous function and the two-dimensional asymptotic crack-tip displacement fields were added to the finite element approximation in [18]. De Borst and et al. [19] investigated discrete and smeared crack models for the concrete fracture. These models were constructed using the partition-of-unity property of the finite element shape functions. A recently developed consecutive-interpolation local enriched partition-of-unity method was used to study quasi-static crack propagation in [20]. Also, Alijani et al. [21] investigated the static behavior of cracked Euler–Bernoulli beam resting on an elastic foundation in which analytical, approximate and numerical approaches were implemented. In the following, Mottaghian et. al [22] developed a new one-dimensional finite element model to investigate the nonlinear elastic response of cracked beams in which a linear rotational spring is used to simulate the crack. Free vibration analysis of an elastically cracked beam was carried out by employing a line spring model to formulate the problem via differential quadrature method by Matbuly and et al.[23]. Nahvi and Jabbari [24] utilized the analytical and the experimental approaches to detect the crack in beams by FEM vibration analysis. Free and forced vibration analyses of a cracked beam were performed via the ANSYS 8.0 finite element program in order to determine the single- and two-edge cracks in a cantilever beam [25]. The free vibration of a shear deformable beam with multiple open edge cracks was studied using a lattice spring model (LSM) by Attar and et al.[26]. Behzad and et al. [27] presented a new continuous model for the vibration analysis of a beam with an open edge crack by using a modified weighted residual method. Shifrin and Ruotolo [28] employed a technique to calculate natural frequencies of a beam with an arbitrary finite number of transverse open cracks. Bachene and et al. [29] implemented the XFEM to analyze the vibrations of cracked plates which was developed for functionally graded material plates in [30]. Nguyen-Thoi and et al. proposed a cell-based smoothed discrete shear gap method (CS-DSG3) using triangular elements for statics and free vibration analyses of Mindlin plates based on XFEM [31].

In this paper, the statics and vibration problems of cracked isotropic bars and beams are investigated by using XFEM. In XFEM analysis, to prevent the complication in the determination of the nodal displacements, a shift function for the enriched nodes is utilized to interpolate the displacement field. In statics analysis, the displacement and modified stiffness matrix are determined for bars and beams via one and two-dimensional models, respectively. Two techniques namely the increasing the number of Gauss integration points and dividing the elements of near crack into sub-grids are implemented to modify the displacement, strain and stress fields. In vibration analysis, an eigenvalue solution is proposed to calculate the natural frequencies and the mode shapes by the improving stiffness and the mass matrices of the beam containing the crack. The effects of depths and positions of the crack, two integration techniques, different boundary conditions and other geometric parameters on the deflection pattern and changes of the natural frequencies and the mode shapes are studied in beams. The validity of the present work is confirmed by the comparison with reported results in references.

2   OVERVIEW OF THE STIFFNESS MATRIX IN THE FINITE ELEMENT METHOD (FEM)

The stiffness matrix is a significant parameter in the finite element analysis. Four steps can be proposed to determine the stiffness matrix for different structures and various phenomena. The kind of element is selected in the first step. One, two or three- dimensional models are initially suggested to simulate problems according to geometric characteristics. In the second step, the shape functions are chosen to interpolate the displacement field. In the third step, the kinematic and constitutive relationships are established to obtain displacement-strain and strain-stress equations, respectively. In the fourth step, the stiffness matrix can be derived using the principle of minimum

potential energy in the combination with the aforementioned steps. In geometrically linear analysis, the variation of strain energy can be reduced [1]

$$\delta U = \int_V \boldsymbol{\sigma} : \delta \boldsymbol{\varepsilon}\, dV = \{\delta \boldsymbol{u}\}^{\mathrm{T}} [\boldsymbol{K}]\{\boldsymbol{u}\} \qquad (1)$$

In which, the stiffness matrix is independent of the displacement.

2.1 FEM in bars

The displacement field is just considered in the axial direction; also no shear force and bending moment are applied in bars. The bar element can be modeled as a one- dimensional element with two nodes in which geometric and material parameters are assumed constant.

The displacement field in each element can be calculated in terms of the nodal displacement and the local coordinate via shape functions [3] as follows:

$$u = \sum_{i=1}^{N^{std}} N_i u_i \qquad (2)$$

Linear shape functions are used to interpolate the axial displacement as:

$$N_i = \frac{1 - \xi_i \xi}{2} \qquad (3a)$$

According to Fig. 1, following equation is used to transform the global coordinate into the parent coordinate

$$\xi = \frac{2}{x_2 - x_1}(x - x_1) - 1 \qquad (3b)$$

The linear displacement-strain relationship in bars is written as:

$$\varepsilon_x = \frac{du}{dx} = \boldsymbol{B}\{\boldsymbol{u}\} \qquad (4a)$$

In which the derivative of shape functions is indicated

$$\boldsymbol{B} = \begin{bmatrix} \dfrac{-1}{L} & \dfrac{1}{L} \end{bmatrix} \qquad (4b)$$

The elastic stress-strain relationship is obtained from [3]

$$\sigma_x = E\,\varepsilon_x \qquad (5)$$

The strain energy equation is written to specify the stiffness matrix

$$U = \frac{1}{2}\int_V \sigma_x^{\,T} \varepsilon_x\, dV = \frac{1}{2}\{\boldsymbol{u}\}^T [\boldsymbol{K}]\{\boldsymbol{u}\} \qquad (6a)$$

By integration with the normally Gauss technique presented in Appendix A, the stiffness matrix is calculated as follows:

$$\boldsymbol{K} = \sum_{p=1}^{N^{Gauss}} \frac{EAL}{2} \left(\boldsymbol{B}^T \boldsymbol{B}\right) w_p = \frac{EA}{L} \begin{bmatrix} 1 & -1 \\ -1 & 1 \end{bmatrix} \tag{6b}$$
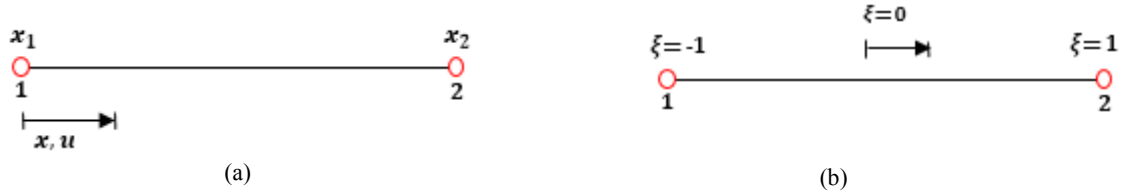

(a)

(b)

Fig.1
One-dimensional element: (a) Global coordinate (b) Parent coordinate.

2.2 FEM in beams

A beam is a slender structure which can be modeled by one and two-dimensional elements in the finite element method. In common theories of the beam like Euler-Bernoulli, Timoshenko and geometrically exact beam, the simulating is carried out by one-dimensional elements, while the isoperimetric formulation based on plane stress or plane strain states is usually utilized to model the beam with two-dimensional elements. Here, the two-dimensional rectangular elements including four nodes are utilized to mesh the beam. According to Fig. 2, the interpolation of the displacement and the position is offered by using the following shape functions [1]

$$N_i = \frac{1}{4}\left(1 + \xi_i \xi\right)\left(1 + \eta_i \eta\right) \tag{7}$$

The linear displacement-strain relationship in plane-stress state is written [3]

$$\left\{\begin{array}{c} \varepsilon_x \\ \varepsilon_y \\ \gamma_{xy} \end{array}\right\} = \left\{\begin{array}{c} \dfrac{\partial u}{\partial x} \\ \dfrac{\partial v}{\partial y} \\ \dfrac{\partial u}{\partial y} + \dfrac{\partial v}{\partial x} \end{array}\right\} = \boldsymbol{B}\left\{\boldsymbol{u}\right\} \tag{8}$$

In reference to Eq. (2), the derivative of the shape functions for each node is

$$\boldsymbol{B}_i^{std} = \begin{bmatrix} \partial N_i / \partial x & 0 \\ 0 & \partial N_i / \partial y \\ \partial N_i / \partial y & \partial N_i / \partial x \end{bmatrix} \tag{9}$$

According to Fig. 2, the following equation is utilized for transforming the global coordinate into the parent coordinate

$$
\begin{Bmatrix} \dfrac{\partial N_i}{\partial x} \\[2mm] \dfrac{\partial N_i}{\partial y} \end{Bmatrix} = \boldsymbol{J}^{-1} \begin{Bmatrix} \dfrac{\partial N_i}{\partial \xi} \\[2mm] \dfrac{\partial N_i}{\partial \eta} \end{Bmatrix}
\tag{10a}
$$

The Jacobian matrix is defined [1]

$$
\boldsymbol{J} = \begin{bmatrix} \dfrac{\partial x}{\partial \xi} & \dfrac{\partial y}{\partial \xi} \\[2mm] \dfrac{\partial x}{\partial \eta} & \dfrac{\partial y}{\partial \eta} \end{bmatrix}
\tag{10b}
$$

The elastic stress-strain relationship is formed from [3]

$$
\sigma = \boldsymbol{D}\varepsilon
\tag{11a}
$$

The isotropic plane-stress stiffness is introduced

$$
\boldsymbol{D} = \frac{E}{1-\vartheta^2} \begin{bmatrix} 1 & \vartheta & 0 \\ \vartheta & 1 & 0 \\ 0 & 0 & \dfrac{1-\vartheta}{2} \end{bmatrix}
\tag{11b}
$$

By substituting Eqs. (9) and (11) into (6a) and using the normally Gauss integration presented in Appendix B, the stiffness matrix related to the nodal combination of i and j within an element is determined

$$
\boldsymbol{K}_{ij} = \int_V \boldsymbol{B}_i^{std\,T} \boldsymbol{D} \boldsymbol{B}_j^{std} \, dV = \int_{-1}^{1}\int_{-1}^{1} t\, \boldsymbol{B}_i^{std\,T} \boldsymbol{D} \boldsymbol{B}_j^{std} \, det\boldsymbol{J} \, d\xi d\eta \approx
$$

$$
\sum_{p=1}^{N^{Guass}} t \left[\boldsymbol{B}_i^{std}\left(\xi_p, \eta_p\right) \right]^T \boldsymbol{D} \left[\boldsymbol{B}_i^{std}\left(\xi_p, \eta_p\right) \right] det\boldsymbol{J}_p w_p
\tag{12}
$$

Fig.2
Two-dimensional element: (a) Global coordinate (b) Parent coordinate.

3   OVERVIEW OF THE STIFFNESS MATRIX IN THE EXTENDED FINITE ELEMENT METHOD

XFEM is a numerical method for modeling discontinuities such as cracks, holes and notched sections which is formulated by combining the standard finite element method and special functions. These functions added to the standard FEM equations are defined based on the type of discontinuity. Two specified function types are generally used to model cracks in structures. One of them is called the *'Heaviside function'* which is used to define the discontinuity during the crack length. The other one assigned as the *'crack tip function'* is efficiently used to estimate the stress concentration effects in the near crack tip. Adding these functions increases the degrees of freedom in nodes of elements around the crack length and tip referred as the *'nodal enrichment'*. In XFEM, the crack is modeled independently from mesh and virtually.

3.1 XFEM in bars

In XFEM analysis, the displacement field is divided into two parts including the standard and the enriched displacement [10]

$$u(x) = u^{std}(x) + u^{enr}(x) \tag{13}$$

The enrichment function is specifically defined as the Heaviside function in the one-dimensional model, so

$$u(x) = \sum_{i=1}^{N_{std}} N_i(x) u_i + \sum_{j=1}^{N_{enr}} N_j(x) H(x) a_j \tag{14}$$

Here, i and j indicate the number of standard and Heaviside enriched nodes, respectively. The Heaviside function is defined as Fig. 3 and following equation

$$H(x) = \begin{cases} 1 & \text{if}(\overline{\mathbf{x}} - \mathbf{x}^*).\mathbf{n} \geq 0 \\ -1 & \text{otherwise} \end{cases} \tag{15}$$

The displacement in each enriched node i can be calculated as:

$$u(x_i) = u_i + H(x_i) a_i \tag{16}$$

The nodal parameter u_i is not the real displacement value in the enriched node [10] so a simple shifting enriched function is used to determine the nodal displacements without involving enriched term. Accordingly, Eq. (14) can be rewritten as:

$$u(x) = \sum_{i=1}^{N_{std}} N_i(x) u_i + \sum_{j=1}^{N_{hev}} N_j(x) \big(H(x) - H(x_j) \big) a_j \tag{17a}$$

In which, Eq. (16) is changed to

$$u(x_i) = u_i \tag{17b}$$

The strain in one-dimensional XEEM is indicated by the use of the shifting enriched function and according to Eq. (4a) as:

$$\varepsilon(x) = \sum_{i=1}^{N^{std}} \frac{\partial N_i(x)}{\partial x} u_i + \sum_{j=1}^{N^{hev}} \left[\frac{\partial N_j(x)}{\partial x} \left(H(x) - H(x_j) \right) + N_j(x) \frac{\partial}{\partial x} \left(H(x) - H(x_j) \right) \right] a_j \qquad (18a)$$

with

$$\frac{\partial}{\partial x} \left(H(x) - H(x_j) \right) = \left(\delta(x) - \delta(x_j) \right) = 0 \qquad (18b)$$

is obtained

$$\varepsilon(x) = \left[\mathbf{B}^{std}(x) \quad \mathbf{B}^{hev}(x) \right] \left\{ \begin{array}{c} \mathbf{u} \\ \mathbf{a} \end{array} \right\} \qquad (18c)$$

and the derivative of the shape functions for each element is achieved as:

$$\mathbf{B} = \left[\frac{-1}{L} \quad \frac{1}{L} \quad \frac{-1}{L} \left(H(x) - H(x_j) \right) \quad \frac{1}{L} \left(H(x) - H(x_{j+1}) \right) \right] \qquad (18d)$$

Substituting Eqs. (18) and (5) into (6a), the stiffness matrix, the displacement and the force vectors are introduced as the following equilibrium equation

$$\begin{bmatrix} \mathbf{K}^{uu} & \mathbf{K}^{ua} \\ \mathbf{K}^{au} & \mathbf{K}^{aa} \end{bmatrix} \left\{ \begin{array}{c} \mathbf{u} \\ \mathbf{a} \end{array} \right\} = \left\{ \begin{array}{c} \mathbf{f}^{u} \\ \mathbf{f}^{a} \end{array} \right\} \qquad (19)$$

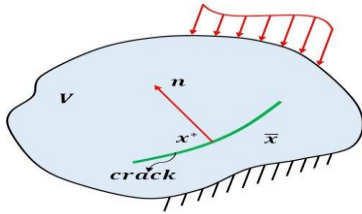In this case, one degree of freedom is enhanced to each enriched node.

Fig.3
Domain *V* of a solid body containing a crack.

3.2 XFEM in beams

Two kinds of the Heaviside and the crack tip enriched functions can be used to model the cracked beams. The Heaviside function is utilized in the element which is completely cut off by the crack. In this case, two extra degrees of freedom are enhanced to each enriched node. The crack tip functions are employed to enrich the element including the crack tip. In this case, eight extra degrees of freedom are added to each enriched node. Other elements of around the crack affected from crack tip and length are partially enriched which are called '*blended elements*', as shown in Fig. 4.

The displacements in each point are determined by the summation of the standard, the Heaviside and the crack tip terms [11]

$$\mathbf{u}(x) = \sum_{i=1}^{N^{std}} N_i(x) u_i + \sum_{j=1}^{N^{hev}} N_j(x) \left(H(x) - H(x_j) \right) a_j + \sum_{k=1}^{N^{tip}} N_k(x) \sum_{\alpha=1}^{4} \left(\beta^\alpha(x) - \beta^\alpha(x_k) \right) b_k \qquad (20)$$

Here, *i, j* and *k* indicate number of the standard, the Heaviside and the crack tip enriched node, respectively, and α is the number of the crack tip functions.

Substituting Eq. (20) into (8), the strain vector can be determined. The Heaviside and the crack tip strains are specified [11]

$$\varepsilon^{enr}\left(\boldsymbol{x}\right)=\boldsymbol{B}^{hev}\left(\boldsymbol{x}\right)\boldsymbol{a}+\boldsymbol{B}^{tip}\left(\boldsymbol{x}\right)\boldsymbol{b} \tag{21a}$$

and

$$\boldsymbol{B}_i^{hev}=\begin{bmatrix} \partial\left(N_i\left(\boldsymbol{x}\right)\left(H\left(\boldsymbol{x}\right)-H\left(\boldsymbol{x}_i\right)\right)\right)\Big/\partial x & 0 \\ 0 & \partial\left(N_i\left(\boldsymbol{x}\right)\left(H\left(\boldsymbol{x}\right)-H\left(\boldsymbol{x}_i\right)\right)\right)\Big/\partial y \\ \partial\left(N_i\left(\boldsymbol{x}\right)\left(H\left(\boldsymbol{x}\right)-H\left(\boldsymbol{x}_i\right)\right)\right)\Big/\partial y & \partial\left(N_i\left(\boldsymbol{x}\right)\left(H\left(\boldsymbol{x}\right)-H\left(\boldsymbol{x}_i\right)\right)\right)\Big/\partial x \end{bmatrix} \tag{21b}$$

$$\boldsymbol{B}_i^{tip\alpha}=\begin{bmatrix} \partial\left(N_i\left(\boldsymbol{x}\right)\left(\beta^\alpha\left(\boldsymbol{x}\right)-\beta^\alpha\left(\boldsymbol{x}_i\right)\right)\right)\Big/\partial x & 0 \\ 0 & \partial\left(N_i\left(\boldsymbol{x}\right)\left(\beta^\alpha\left(\boldsymbol{x}\right)-\beta^\alpha\left(\boldsymbol{x}_i\right)\right)\right)\Big/\partial y \\ \partial\left(N_i\left(\boldsymbol{x}\right)\left(\beta^\alpha\left(\boldsymbol{x}\right)-\beta^\alpha\left(\boldsymbol{x}_i\right)\right)\right)\Big/\partial y & \partial\left(N_i\left(\boldsymbol{x}\right)\left(\beta^\alpha\left(\boldsymbol{x}\right)-\beta^\alpha\left(\boldsymbol{x}_i\right)\right)\right)\Big/\partial x \end{bmatrix} \alpha=1,2..,4 \tag{21c}$$

In which according to Fig. 5, the crack tip functions are introduced in the local and polar coordinates [10] as:

$$\beta(r,\theta)=\left\{\sqrt{r}\sin\left(\frac{\theta}{2}\right),\sqrt{r}\cos\left(\frac{\theta}{2}\right),\sqrt{r}\,\sin(\theta)\sin\left(\frac{\theta}{2}\right),\sqrt{r}\,\sin(\theta)\cos\left(\frac{\theta}{2}\right)\right\} \tag{21d}$$

According to Eq. (19), the stiffness matrix related to the nodal combination of i and j, the nodal displacement and the force vectors can be determined by substituting Eq. (21) into Eqs. (11) and (12), ten extra degrees of freedom are added to each enriched node, so $\boldsymbol{K}_{ij}$ possesses the size 12×12.

$$\boldsymbol{K}_{ij}=\begin{bmatrix} \boldsymbol{K}_{ij}^{uu} & \boldsymbol{K}_{ij}^{ua} & \boldsymbol{K}_{ij}^{ub} \\ \boldsymbol{K}_{ij}^{au} & \boldsymbol{K}_{ij}^{aa} & \boldsymbol{K}_{ij}^{ab} \\ \boldsymbol{K}_{ij}^{bu} & \boldsymbol{K}_{ij}^{ba} & \boldsymbol{K}_{ij}^{bb} \end{bmatrix} \tag{22a}$$

$$F_i=\begin{Bmatrix} \boldsymbol{f}^{u} \\ \boldsymbol{f}^{a} \\ \boldsymbol{f}^{b} \end{Bmatrix}_i \tag{22b}$$

$$\{\boldsymbol{u}\}_i=\begin{Bmatrix} \boldsymbol{u} \\ \boldsymbol{a} \\ \boldsymbol{b} \end{Bmatrix}_i \tag{22c}$$

where,

$$
\mathbf{K}_{ij} = \begin{bmatrix}
\int_V \left(\mathbf{B}_i^{std}\right)^T \mathbf{DB}_j^{std}\,dV & \int_V \left(\mathbf{B}_i^{std}\right)^T \mathbf{DB}_j^{hev}\,dV & \int_V \left(\mathbf{B}_i^{std}\right)^T \mathbf{DB}_j^{tip\,\alpha}\,dV \\
\int_V \left(\mathbf{B}_i^{hev}\right)^T \mathbf{DB}_j^{std}\,dV & \int_V \left(\mathbf{B}_i^{hev}\right)^T \mathbf{DB}_j^{hev}\,dV & \int_V \left(\mathbf{B}_i^{hev}\right)^T \mathbf{DB}_j^{tip\,\alpha}\,dV \\
\int_V \left(\mathbf{B}_i^{tip\,\alpha}\right)^T \mathbf{DB}_j^{std}\,dV & \int_V \left(\mathbf{B}_i^{tip\,\alpha}\right)^T \mathbf{DB}_j^{hev}\,dV & \int_V \left(\mathbf{B}_i^{tip\,\alpha}\right)^T \mathbf{DB}_j^{tip\,\alpha}\,dV
\end{bmatrix}
\tag{22d}
$$

The nodal force vector for a cracked structure under traction force can be calculated as:

$$
\mathbf{F}_i = \begin{bmatrix}
\int_\Gamma \left(N_i^{std}\right)^T t_f\,d\Gamma \\
\int_\Gamma \left(N_i^{hev}\right)^T t_f\,d\Gamma \\
\int_\Gamma \left(N_i^{tip\,\alpha}\right)^T t_f\,d\Gamma
\end{bmatrix}
\tag{22e}
$$

Here,

$$
N_i^{std} = N_i\left(\mathbf{x}\right)
\tag{22f}
$$

$$
N_i^{hev} = N_i\left(\mathbf{x}\right)\left(H\left(\mathbf{x}\right) - H\left(\mathbf{x}_i\right)\right)
\tag{22g}
$$

$$
N_i^{tip\,\alpha} = N_i\left(\mathbf{x}\right)\left(\beta^\alpha\left(\mathbf{x}\right) - \beta^\alpha\left(\mathbf{x}_i\right)\right)
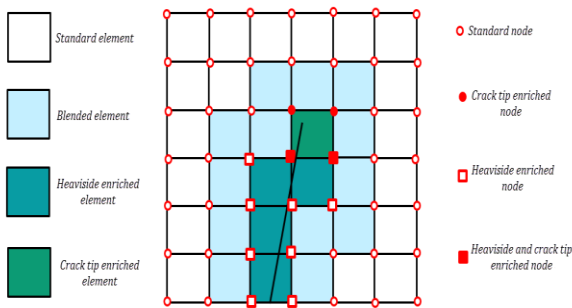\tag{22h}
$$

Fig.4
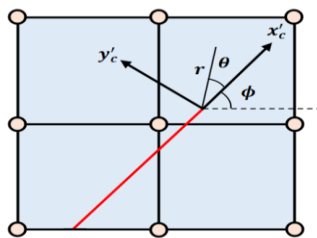Two-dimensional standard, blended and enriched elements.

Fig.5
Local and polar coordinate of crack tip.

4　INTEGRATION TECHNIQUES

The polynomial shape functions are commonly used to interpolate in the quadratic standard elements. The normally Gauss integration technique in such problems can be implemented to obtain acceptable results. On the other side, the enhanced terms in XFEM may create non-polynomial and non-smooth functions, so one of the important and complex problems is the integration within the enriched elements. Due to considerable variations of parameters in the crack region, using the normally Gauss integration technique may lead to ill condition for stiffness matrix and inappropriate numerical results. Increasing the number of Gauss points is proposed as a conventional technique to remedy these poor results. Another alternatively useful technique for numerical integration is adopted by dividing the enriched and the blended elements into smaller elements called the *'sub-grid elements'*. This technique is only employed for numerical integration without adding any extra degrees of freedom. These three techniques are illustrated in Fig. 6.
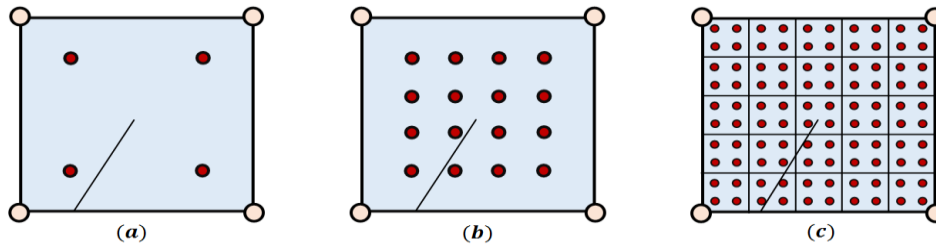

Fig.6
Different integration techniques: (a) Normally Gauss integration technique (b) Gauss integration technique with 16 points (c) Sub-grid technique.

4.1 FEM in bars via the sub-grid technique

For the investigating of the sub-grid concept in FEM, one standard element of the bar is divided into two sub-grids according to Fig. 7. The strain energy of this element is computed by the energies summation of two sub-grids.

$$U_{element} = \sum_{k=1}^{N^{sub}} U_{sub}{}^{k} \tag{23}$$

The strain energy in the left sub-grid can be determined according to Eq. (6a) as:

$$U_L = \frac{1}{2}\int_0^{x_0} EA\left(\frac{\partial u_L(x)}{\partial x}\right)^T \left(\frac{\partial u_L(x)}{\partial x}\right) dx \tag{24}$$

The left sub-grid displacement field can be interpolated according to Eq. (2)

$$u_L = N_1{}^L u_1 + N_2{}^L u_2 \tag{25}$$

The derivative of the shape functions of the left sub-grid is achieved according to Eq. (4b) as:

$$\boldsymbol{B}_L = \begin{bmatrix} \dfrac{-1}{x_0} & \dfrac{1}{x_0} \end{bmatrix} \tag{26}$$

The left sub-grid strain energy is calculated in terms of the displacements of the sub-grid as:

$$U_L = \frac{1}{2}\{u_L\}^T [k_L]\{u_L\} = \frac{1}{2}\{u_1 u_2\}[k_L]\begin{Bmatrix} u_1 \\ u_2 \end{Bmatrix}$$ (27a)

In which, the left sub-grid stiffness matrix is obtained according to Eq. (6b)

$$[k_L] = \frac{EA}{x_0}\begin{bmatrix} 1 & -1 \\ -1 & 1 \end{bmatrix}$$ (27b)

By the same analysis, the right sub-grid strain energy can be evaluated as:

$$U_R = \frac{1}{2}\{u_R\}^T [k_R]\{u_R\} = \frac{1}{2}\{u_2 u_3\}[k_R]\begin{Bmatrix} u_2 \\ u_3 \end{Bmatrix}$$ (28a)

The right sub-grid stiffness is introduced

$$[k_R] = \frac{EA}{L - x_0}\begin{bmatrix} 1 & -1 \\ -1 & 1 \end{bmatrix}$$ (28b)

The nodal displacement vector of the basic element can be connected to the sub-grids nodal displacement vector as:

$$\{u_L\} = C_L \{u\}$$ (29a)

$$\{u_R\} = C_R \{u\}$$ (29b)

In which

$$C_L = \begin{bmatrix} 1 - \dfrac{x_1}{L} & \dfrac{x_1}{L} \\ 1 - \dfrac{x_2}{L} & \dfrac{x_2}{L} \end{bmatrix}$$ (29c)

$$C_R = \begin{bmatrix} 1 - \dfrac{x_2}{L} & \dfrac{x_2}{L} \\ 1 - \dfrac{x_3}{L} & \dfrac{x_3}{L} \end{bmatrix}$$ (29d)

Here, C_L and C_R are called as *'the conversion matrices'* for the left and right sub-grids, respectively. By using the conversion matrices, Eqs. (27) and (28) can be rewritten as:

$$U_L = \frac{1}{2}\{u\}^T [C_L]^T [k_L][C_L]\{u\} \Rightarrow K_L = [C_L]^T [k_L][C_L]$$ (30a)

$$U_R = \frac{1}{2}\{u\}^T [C_R]^T [k_R][C^R]\{u\} \Rightarrow K_R = [C_R]^T [k_R][C_R]$$ (30b)

According to Eqs. (23), the stiffness matrix of the basic element can be determined by the sum of the two sub-grids stiffness matrices

$$K_{element} = \sum_{k=1}^{N^{sub}} K_{sub}{}^{k} = K_L + K_R \tag{31}$$
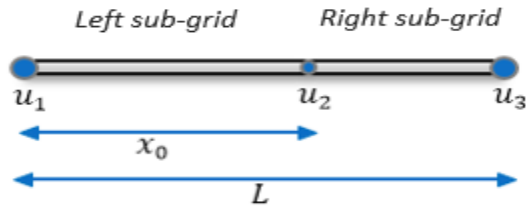

Fig.7
Sub-grid for intact bar element**.**

4.2 XFEM in bars via the sub-grid technique

In this analysis, two types of elements are defined to develop the governing equations of bars. One is the standard elements and another is the elements containing the discontinuity enriched by the Heaviside function. It is assumed that the enriched elements are divided into three sub-grids including the crack length, the left side and the right side of the crack as Fig. 8. In reference to Eq. (23), the strain energy of the basic element is given

$$U_{element} = \sum_{k=1}^{3} \frac{1}{2} \{u^k\}^T \left[k_{sub}{}^k\right] \{u^k\} \tag{32a}$$

In reference to Eq. (6b), the stiffness matrix for each sub-grid element of length $L/3$ can be determined as:

$$k_{sub}^k = \frac{3AE}{L} \begin{bmatrix} 1 & -1 \\ -1 & 1 \end{bmatrix} \tag{32b}$$

As mentioned, the nodal displacements of each sub-grid element can be connected to the nodal displacement vector of the basic element as:

$$\{u^k\} = \sum_{i=1}^{2} \left[\left(C_{sub}{}^k\right)_i\right] \{u^e\}_i \tag{33a}$$

The nodal displacement vectors of each sub-grid and basic elements are introduced as:

$$\{u^k\} = \begin{Bmatrix} u_1^k \\ u_2^k \end{Bmatrix} \tag{33b}$$

$$\{u^e\}_i = \begin{Bmatrix} u \\ a \end{Bmatrix}_i \tag{33c}$$

The conversion matrix which contains two parts of the standard and Heaviside is obtained

$$\left(C_{sub}{}^k\right)_i = \left[C_i^{std}, C_i^{hev}\right] \tag{34a}$$

In which

$$C_i^{std} = \begin{bmatrix} N_i\left(x_1^{\,k}\right) \\ N_i\left(x_2^{\,k}\right) \end{bmatrix}$$

(34b)

$$C_i^{hev} = \begin{bmatrix} N_i\left(x_1^{\,k}\right)\left(H\left(x^k\right) - H\left(x_i\right)\right) \\ N_i\left(x_2^{\,k}\right)\left(H\left(x^k\right) - H\left(x_i\right)\right) \end{bmatrix}$$

(34c)

Based on the position of the crack and Eq. (15), the Heaviside function value in the first and second nodes of basic element is computed as:

$$H\left(x_{i=1}\right) = -1 \qquad H\left(x_{i=2}\right) = 1$$

(34d)

By considering Eqs. (27) and (28), the strain energy for each sub-grid can be rewritten

$$U_{sub}^{\,k} = \frac{1}{2}\left\{\boldsymbol{u}^e\right\}^T \left[\boldsymbol{C}_{sub}^{\,k}\right]^T \left[\boldsymbol{k}_{sub}^{\,k}\right]\left[\boldsymbol{C}_{sub}^{\,k}\right]\left\{\boldsymbol{u}^e\right\}$$

(35a)

So, the improved sub-grid stiffness matrix is achieved as:

$$\boldsymbol{K}_{sub}^{\,k} = \left[\boldsymbol{C}_{sub}^{\,k}\right]^T \left[\boldsymbol{k}_{sub}^{\,k}\right]\left[\boldsymbol{C}_{sub}^{\,k}\right]$$
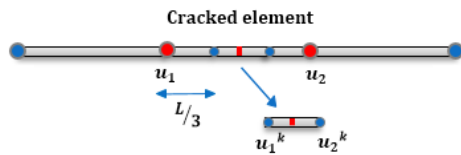
(35b)

Fig.8
Sub-gird for cracked bar element.

4.3 XFEM in beams via the sub-grid technique

As indicated in section 3.2, for the cracked beam analysis, the elements are divided into three parts as the standard, the blended and the cracked elements enriched by the Heaviside and the crack tip functions. For employing the sub-grid technique, the blended and the enriched elements should be divided into some sub-grids as Fig. 6. According to Eq. (23), the strain energy of each blended or enriched element can be determined as the energies summation of the sub-grids as:

$$U_{element} = \sum_{k=1}^{N^{sub}} \frac{1}{2}\left\{\boldsymbol{u}^k\right\}^T \left[\boldsymbol{k}_{sub}^{\,k}\right]\left\{\boldsymbol{u}^k\right\}$$

(36)

Here, the stiffness matrix for each sub-grid can be calculated as Eq.(12). According to Eq. (33a), in a two-dimensional analysis, the nodal displacements of each sub-grid element can be defined in terms of the nodal displacements of the basic element as:

$$\left\{\boldsymbol{u}^k\right\} = \sum_{i=1}^{4} \left[\left(\boldsymbol{C}_{sub}^{\,k}\right)_i\right]\left\{\boldsymbol{u}^e\right\}_i$$

(37a)

The nodal displacement vectors of each sub-grid and the basic elements are indicated as:

$$\left\{ u^k \right\}^T = \left\{ u_1^{\ k} \quad v_1^{\ k} \quad u_2^{\ k} \quad v_2^{\ k} \quad u_3^{\ k} \quad v_3^{\ k} \quad u_4^{\ k} \quad v_4^{\ k} \right\}$$

(37b)

$$\left\{ u^e \right\}^T_i = \left\{ u \quad v \quad a_x \quad a_y \quad b_{1x} \quad b_{1y} \quad b_{2x} \quad b_{2y} \quad b_{3x} \quad b_{3y} \quad b_{4x} \quad b_{4y} \right\}_i$$

(37c)

So, the conversion matrix includes three parts of the standard, the Heaviside and the crack tip. This matrix can be formed for each node as:

$$\left(C_{sub}^{\ k} \right)_i = \left[C_i^{\ std}, C_i^{\ hev}, C_i^{\ tip \ \alpha} \right]$$

(38a)

In which, each part of the coversion matrix is obtained from

$$C_i^{\ std} = \begin{bmatrix} N_i \left(x_1^{\ k} \right) & 0 \\ 0 & N_i \left(x_1^{\ k} \right) \\ N_i \left(x_2^{\ k} \right) & 0 \\ 0 & N_i \left(x_2^{\ k} \right) \\ N_i \left(x_3^{\ k} \right) & 0 \\ 0 & N_i \left(x_3^{\ k} \right) \\ N_i \left(x_4^{\ k} \right) & 0 \\ 0 & N_i \left(x_4^{\ k} \right) \end{bmatrix}$$

(38b)

$$C_i^{\ hev} = \begin{bmatrix} N_i \left(x_1^{\ k} \right) \left(H \left(x^k \right) - H \left(x_i \right) \right) & 0 \\ 0 & N_i \left(x_1^{\ k} \right) \left(H \left(x^k \right) - H \left(x_i \right) \right) \\ N_i \left(x_2^{\ k} \right) \left(H \left(x^k \right) - H \left(x_i \right) \right) & 0 \\ 0 & N_i \left(x_2^{\ k} \right) \left(H \left(x^k \right) - H \left(x_i \right) \right) \\ N_i \left(x_3^{\ k} \right) \left(H \left(x^k \right) - H \left(x_i \right) \right) & 0 \\ 0 & N_i \left(x_3^{\ k} \right) \left(H \left(x^k \right) - H \left(x_i \right) \right) \\ N_i \left(x_4^{\ k} \right) \left(H \left(x^k \right) - H \left(x_i \right) \right) & 0 \\ 0 & N_i \left(x_4^{\ k} \right) \left(H \left(x^k \right) - H \left(x_i \right) \right) \end{bmatrix}$$

(38c)

$$\boldsymbol{C}_i^{tip\,\alpha} = \begin{bmatrix} N_i\left(\boldsymbol{x}_1{}^k\right)\left(\beta^\alpha\left(\boldsymbol{x}^k\right)-\beta^\alpha\left(\boldsymbol{x}_i\right)\right) & 0 \\ 0 & N_i\left(\boldsymbol{x}_1{}^k\right)\left(\beta^\alpha\left(\boldsymbol{x}^k\right)-\beta^\alpha\left(\boldsymbol{x}_i\right)\right) \\ N_i\left(\boldsymbol{x}_2{}^k\right)\left(\beta^\alpha\left(\boldsymbol{x}^k\right)-\beta^\alpha\left(\boldsymbol{x}_i\right)\right) & 0 \\ 0 & N_i\left(\boldsymbol{x}_2{}^k\right)\left(\beta^\alpha\left(\boldsymbol{x}^k\right)-\beta^\alpha\left(\boldsymbol{x}_i\right)\right) \\ N_i\left(\boldsymbol{x}_3{}^k\right)\left(\beta^\alpha\left(\boldsymbol{x}^k\right)-\beta^\alpha\left(\boldsymbol{x}_i\right)\right) & 0 \\ 0 & N_i\left(\boldsymbol{x}_3{}^k\right)\left(\beta^\alpha\left(\boldsymbol{x}^k\right)-\beta^\alpha\left(\boldsymbol{x}_i\right)\right) \\ N_i\left(\boldsymbol{x}_4{}^k\right)\left(\beta^\alpha\left(\boldsymbol{x}^k\right)-\beta^\alpha\left(\boldsymbol{x}_i\right)\right) & 0 \\ 0 & N_i\left(\boldsymbol{x}_4{}^k\right)\left(\beta^\alpha\left(\boldsymbol{x}^k\right)-\beta^\alpha\left(\boldsymbol{x}_i\right)\right) \end{bmatrix} \tag{38d}$$

Substituting Eqs. (37), (38) into (36), the strain energy for each sub-grid in terms of basic nodes is determined as:

$$U_{sub}{}^k = \frac{1}{2}\{\boldsymbol{u}^e\}^T \left[\boldsymbol{C}_{sub}{}^k\right]^T \left[\boldsymbol{k}_{sub}{}^k\right]\left[\boldsymbol{C}_{sub}{}^k\right]\{\boldsymbol{u}^e\} \tag{39a}$$

In which, the improved sub-grid stiffness matrix is computed as:

$$\boldsymbol{K}_{sub}{}^k = \left[\boldsymbol{C}_{sub}{}^k\right]^T \left[\boldsymbol{k}_{sub}{}^k\right]\left[\boldsymbol{C}_{sub}{}^k\right] \tag{39b}$$

5 FREE VIBRATION ANALYSIS IN TWO-DIMENSIONAL XFEM

A free vibration analysis in XFEM can be established by adding the enriched functions into the stiffness and the mass matrices. Constructing the mass matrix is completed by enhancing the shape functions of the Heaviside and the crack tip. This enhanced shape function matrix can be defined for each blended and enriched node as:

$$\boldsymbol{N}_i = \begin{bmatrix} \boldsymbol{N}_i{}^{std}, \boldsymbol{N}_i{}^{hev}, \boldsymbol{N}_i{}^{tip\,\alpha} \end{bmatrix} \tag{40a}$$

In which

$$\boldsymbol{N}_i^{std} = \begin{bmatrix} N_i\left(\boldsymbol{x}\right) & 0 \\ 0 & N_i\left(\boldsymbol{x}\right) \end{bmatrix} \tag{40b}$$

$$N_i^{hev} = \begin{bmatrix} N_i\left(\boldsymbol{x}\right)\left(H\left(\boldsymbol{x}\right)-H\left(\boldsymbol{x}_j\right)\right) & 0 \\ 0 & N_i\left(\boldsymbol{x}\right)\left(H\left(\boldsymbol{x}\right)-H\left(\boldsymbol{x}_i\right)\right) \end{bmatrix} \tag{40c}$$

$$N_i^{tip\,\alpha} = \begin{bmatrix} N_i\left(\boldsymbol{x}\right)\left(\beta^\alpha\left(\boldsymbol{x}\right)-\beta^\alpha\left(\boldsymbol{x}_k\right)\right) & 0 \\ 0 & N_i\left(\boldsymbol{x}\right)\left(\beta^\alpha\left(\boldsymbol{x}\right)-\beta^\alpha\left(\boldsymbol{x}_i\right)\right) \end{bmatrix} \tag{40d}$$

The mass matrix in FEM is defined as [4] and [1]

$$M_{ij} = \int_V \rho (N_i)^T (N_j) dV \tag{41}$$

Substituting the shape function matrix into Eq. (41), the mass matrix related to the nodal combination of i and j within an element in XFEM is assigned as:

$$M_{ij} = \begin{bmatrix} M_{ij}^{uu} & M_{ij}^{ua} & M_{ij}^{ub} \\ M_{ij}^{au} & M_{ij}^{aa} & M_{ij}^{ab} \\ M_{ij}^{bu} & M_{ij}^{ba} & M_{ij}^{bb} \end{bmatrix} \tag{42}$$

The natural frequency is obtained by substituting the enriched stiffness and the mass matrices into the eigenvalue equation [5]

$$\left\| \left([K] - \{\omega^2\}[M] \right) \right\| = 0 \tag{43}$$

Here, *K* and *M* are total stiffness and mass matrices.

6   RESULTS AND DISCUSSION

The effects of the crack on results of statics and vibration analyses of the beams are investigated according to the aforementioned formulations by using some case studies. Different boundary conditions including simply supported-simply supported (SS-SS), clamped-free (C-F) and clamped-clamped (C-C) are considered for a beam with material properties $E = 30\ GPa,\ \vartheta = 0.3,\ \rho = 7850 kg / m^3$ and geometrical parameters shown in Fig. 9. In the statics analysis, the deformation pattern and the stress contours under a uniformly distributed force are evaluated for various crack depths and positions. In the vibration analysis, changes of the natural frequencies and the mode shapes due to a crack are studied.

Results of Fig.10 confirm a convergence in the XFEM analysis. This figure depicted for a two-dimensional beam shows that by increasing the number of elements (after about 189 elements), a negligible change is seen between the obtained results.

A comparison in Fig.11 is drawn to validate the results. This figure depicts a close agreement (about 4% error) between the results of the present work and Abaqus software.
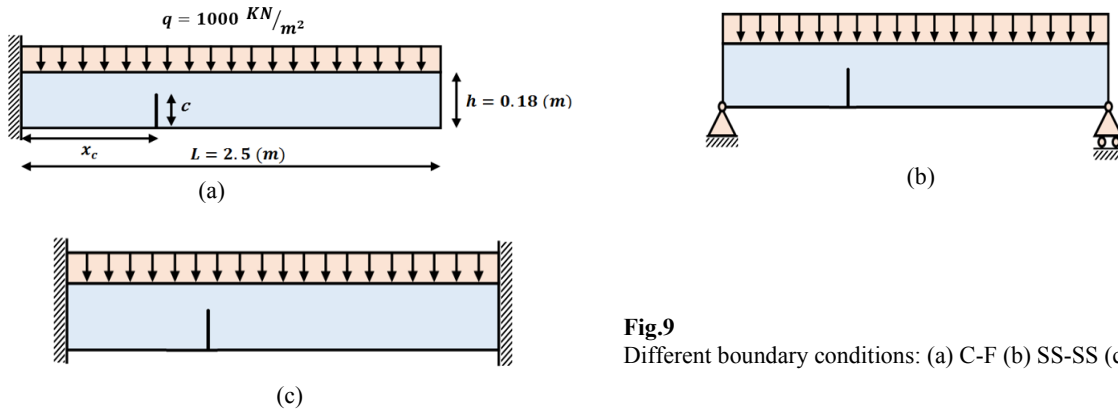

Fig.9
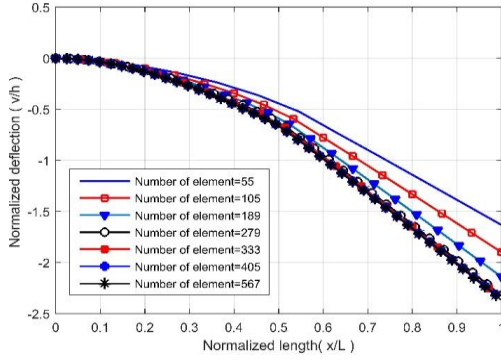Different boundary conditions: (a) C-F (b) SS-SS (c) C-C.

Fig.10
Convergence rate for a C-F beam containing a crack on $x_c/L = 1/2$ and $c/h = 1/2$.
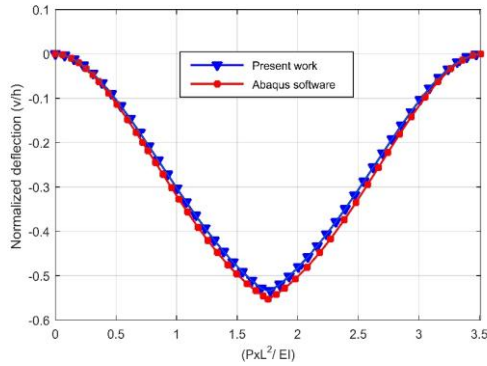

Fig.11
Comparison of the deflection in present work and Abaqus software for C-C cracked beam at $x_c/L = 1/2$ and $c/h = 1/2$.

6.1 Statics analysis

Table 1. shows the maximum deflection of the cracked beam determined with the three different techniques of the normally Gauss integration, the increase of the number of Gauss integration points and the rectangular sub-grid. The normally Gauss integration technique is defined with 4 Gauss points located within each enriched element. 16 Gauss points, see Appendix B, for elements around the crack are selected in the technique of increasing the number of Gauss integration points. In the sub-grid technique, the enriched and blended elements are divided into 49 (7×7) sub-grids with 4 Gauss points within each sub-grid.

By considering non-polynomial shape functions in XFEM, poor results are achieved by using the normally Gauss integration technique. This table confirms that accuracy of the integration can be improved by adding Gauss points. In order to obtain a more appropriate outcome, the sub-grid technique is implemented. The effects of discontinuity along the crack and the singularity at the crack tip are diminished by using this technique in which more computational effort is required in comparison with the other techniques. So, the results of the present work are derived based on the rectangle sub-grid technique. Since the assumed distributed force in the C-C beams generates small deflections; the minor influence of the sub-grid technique on the results of this boundary condition can be recognized in Table1.

The effects of the crack position on the deflection are demonstrated in Figs. 12(a), 12(b) and 12(c) for C-F, SS-SS and C-C B.C., respectively. Here, the crack depth is considered as $c/h = 1/2$. Fig. 12(a) illustrates that more deflection can be observed as the crack positions closer to the clamped support, while for Figs. 12(b) and 12(c), more deflection can be seen if the crack approaches to the middle of the beam. Also, a symmetry in the deflection patterns about the beam center is observed between the crack position at $L/3$ and $2L/3$. In a constant crack depth like $c/h = 1/2$, ratios of the maximum deflection between the cracked and the perfect beam are diversely found in terms of crack positions and boundary conditions. It means that in $x_c/L = 1/2$, these ratios are computed 19%, 41%

and 89% for C-F, C-C and SS-SS B.C., respectively, while these ratios are achieved 78%, 1.4% and 25.3% at $x_c/L = 1/5$.

In Fig. 13, the effect of crack the depth on the deflection is illustrated by considering three different crack depths in a constant crack position $x_c/L = 1/2$. It is obviously observed that the deflection increases by raising the crack depth for all boundary conditions. Based on these figures, SS-SS B.C. possess the widest variation range of deflection with increasing the crack depth. In other words, for SS-SS B.C, the maximum deflection in the presence of the crack at $c/h = 1/2$ increases 89% in comparison with the perfect beam, while this value increases 41% and 19% in C-C and C-F B.C., respectively.

Table 1
Maximum deflection in the cracked beam with three different techniques.

(a) C-F B.C.

x_c/L	c/h	Gauss No	4	16	4
		sub-grid No	1-1	1-1	7-7
$1/5$	$1/2$		0.6509	0.6023	0.5928
$1/3$	$1/2$		0.5228	0.4917	0.4850
$1/2$	$1/2$		0.4198	0.3991	0.3970
$2/3$	$1/2$		0.3564	0.3531	0.3527
$1/2$	$1/3$		0.3715	0.3639	0.3620
$1/2$	$1/6$		0.3534	0.3464	0.3461

(b) SS-SS B.C.

x_c/L	c/h	Gauss No	4	16	4
		sub-grid No	1-1	1-1	7-7
$1/5$	$1/2$		0.0462	0.0444	0.0441
$1/3$	$1/2$		0.0631	0.0578	0.0567
$1/2$	$1/2$		0.0780	0.0677	0.0667
$2/3$	$1/2$		0.0607	0.0565	0.0560
$1/2$	$1/3$		0.0541	0.0503	0.0494
$1/2$	$1/6$		0.0450	0.0417	0.0416

(c) C-C B.C.

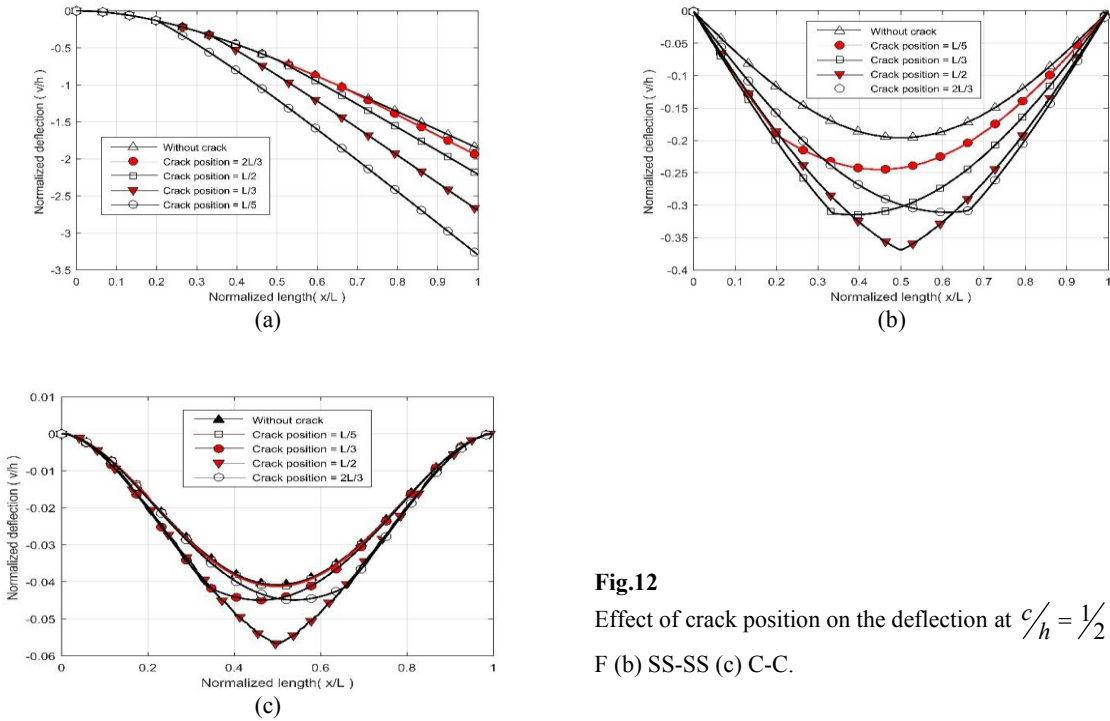| x_c/L	c/h	Gauss No	4	16	4
		sub-grid No	1-1	1-1	7-7
$1/5$	$1/2$		0.0074	0.0074	0.0074
$1/3$	$1/2$		0.0082	0.0081	0.0081
$1/2$	$1/2$		0.0107	0.0103	0.0103
$2/3$	$1/2$		0.0081	0.0080	0.0080
$1/2$	$1/3$		0.0096	0.0092	0.0092
$1/2$	$1/6$		0.0087	0.0083	0.0083

(a)

(b)

(c)

Fig.12

Effect of crack position on the deflection at $c/h = 1/2$: (a) C-F (b) SS-SS (c) C-C.
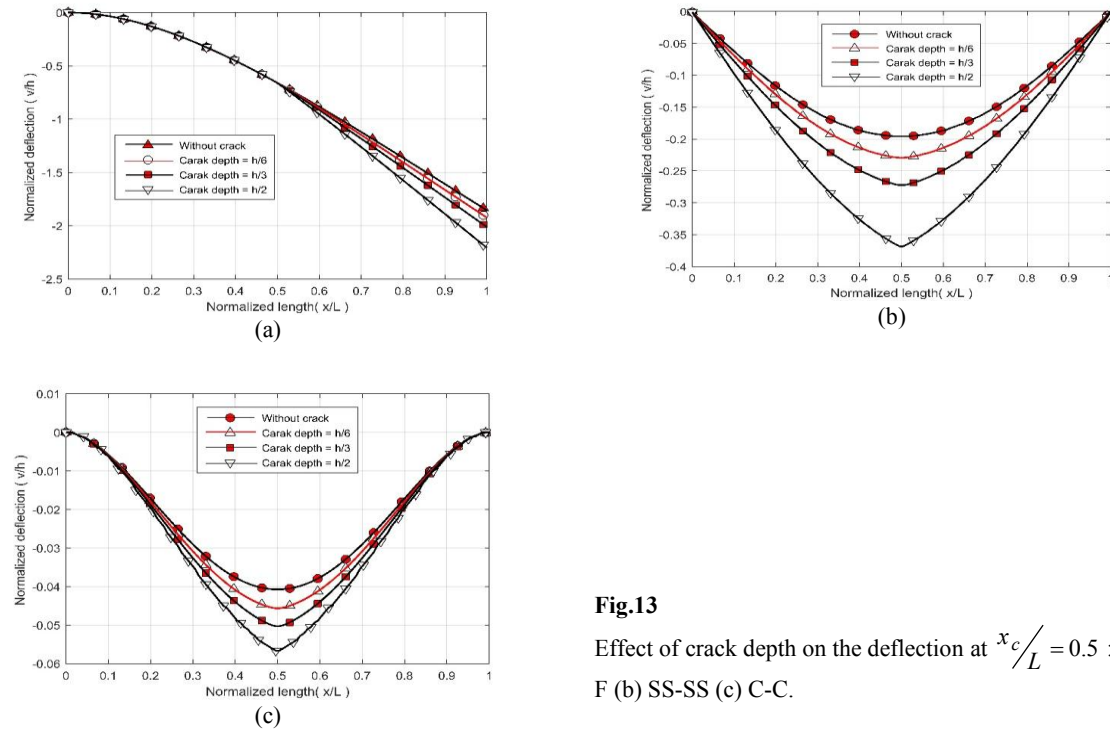

(a)

(b)

(c)

Fig.13

Effect of crack depth on the deflection at $x_c/L = 0.5$: (a) C-F (b) SS-SS (c) C-C.

The estimation of stress contours for beams containing a crack at $x_c/L = 1/2$ or $x_c/L = 1/4$ with $c/h = 1/2$ is indicated in Figs. 14 and 15, respectively. It is noticed that the maximum stress is created around the crack tip. In the other words, there is a stress concentration near the crack. With considering Figs. 14(a) and 14(b), a relative equality in values of maximum and minimum stresses is observed between C-F and SS-SS B.C , while according to Figs. 15(a)and 15(b), these stress values increase (decrease) in C-F (SS-SS) B.C. With the comparison of Figs. 14(c) and

15(c), a negligible variation is seen in the values of maximum and minimum stresses for C-C boundary conditions, while the stress concentration around the crack in Fig.14(c) significantly changes in comparing with Fig.15(c).

(a)

(b)

(c)
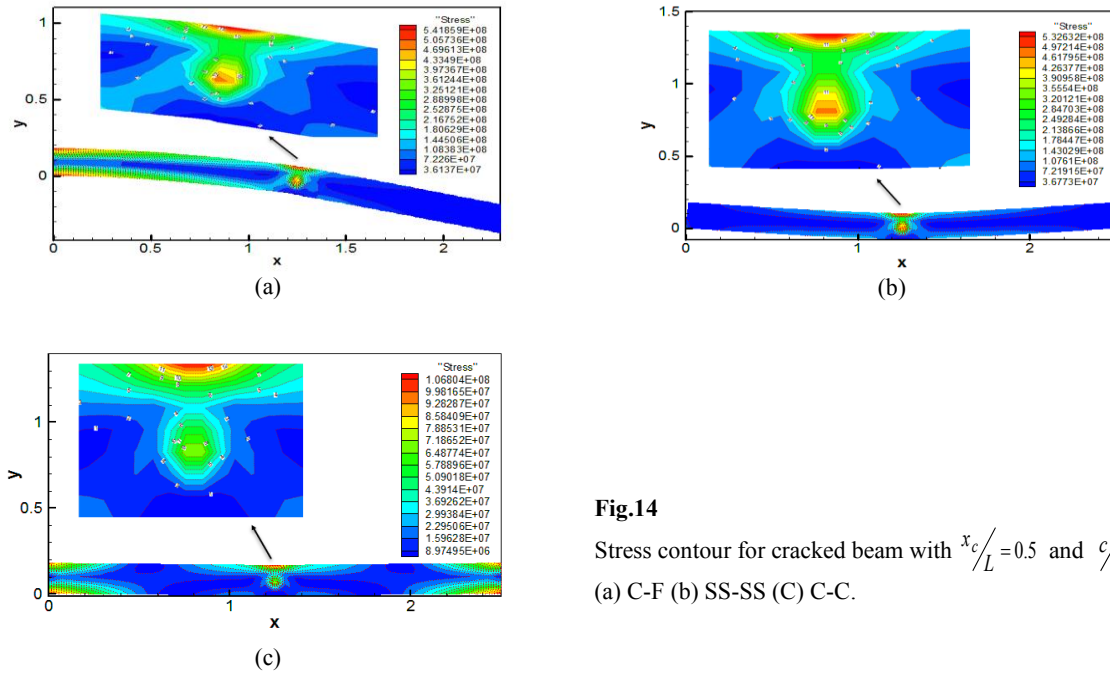
Fig.14

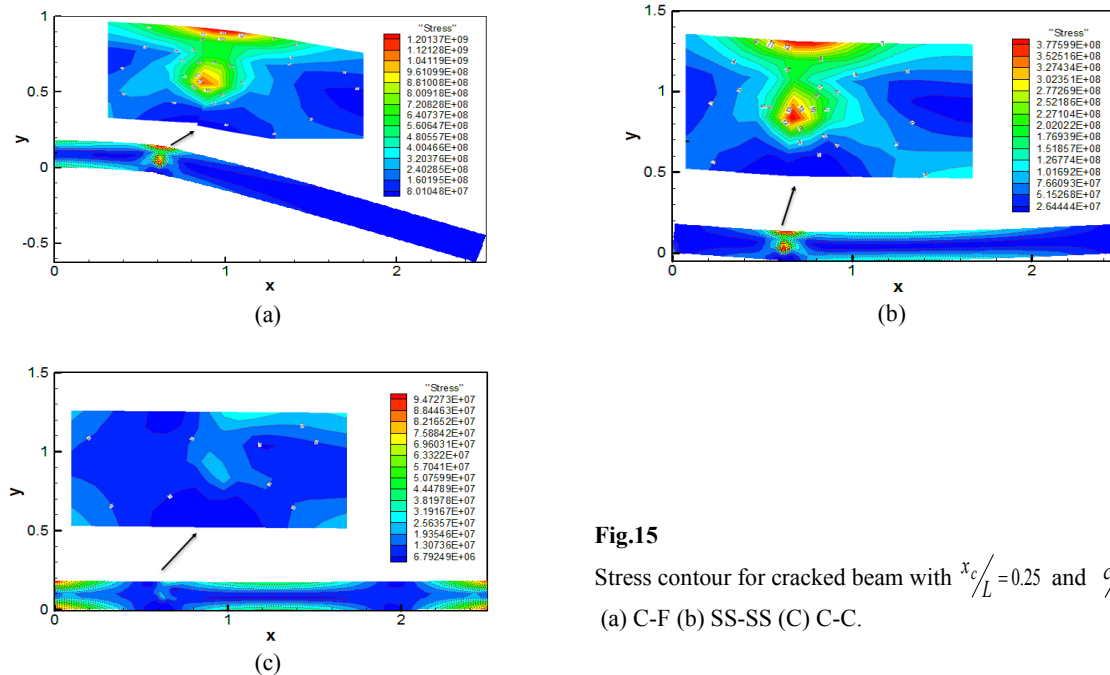Stress contour for cracked beam with $x_c/L = 0.5$ and $c/h = 0.5$
(a) C-F (b) SS-SS (C) C-C.

(a)

(b)

(c)

Fig.15

Stress contour for cracked beam with $x_c/L = 0.25$ and $c/h = 0.5$
(a) C-F (b) SS-SS (C) C-C.

6.2 Free vibration analysis

In this section, the effects of different crack positions and depths are investigated on the mode shapes and the natural frequencies in C-F, SS-SS and C-C boundary conditions. Fig. 16 shows the influence of crack position on the first natural frequency ratio between the cracked beam and perfect beam. This figure confirms the verification of the results of the free vibration analysis. The fewer values in the results of present work illustrate the effects of full

crack simulation in the XFEM analysis. This simulation is performed by considering the discontinuity and the crack tip functions, while Shifrin and Ruotolo [27] adopted a rotational spring model for the simulation the crack. This nearly complete simulation the indicates that the natural frequency ratio of Ref. [27] is computed with the greatest difference about 6% in the comparison with the present work.

Fig. 17 demonstrates the influence of the crack position on the first natural frequency for various crack depths in the three boundary conditions. Fig. 17(a) shows that the influence of the crack depth is negligible where the crack position is close to the free end. It means for all crack depths in C-F B.C, values of the natural frequency are nearly estimated 57 ($\frac{1}{s}$). As the crack positions closer to the clamped support, the fewer values of the natural frequency are observed. By increasing the crack depth, these values reduce in all crack positions.

According to Fig. 17(b) depicted for SS-SS B.C., the minimum natural frequency in each crack depth is observed where the crack sits at the middle of the beam. Increasing the crack depth leads to the decrease of natural frequencies values similar to C-F boundary conditions. The maximum natural frequency is achieved where the crack is located near to the supports.

Fig. 17(c) emphasizes the increase of the crack depth results in the decrease of the natural frequency for C-C B.C. the minimum value of the natural frequency is found for each crack depth where the crack position is at the middle of the beam. The maximum value of the natural frequency in each crack depth is roughly estimated where the crack position sits at $\frac{x_c}{L}$ =0.22 or 0.78. It is noticed that for these two positions, the effect of crack depth can be ignored on the determination of the natural frequency. In other words, the difference of these natural frequencies is 2.42%.
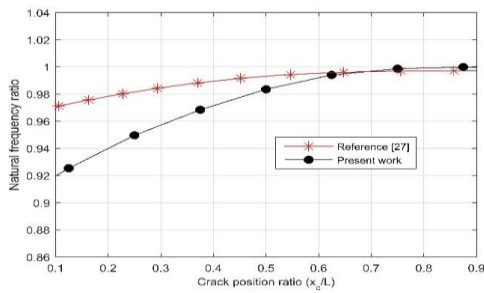

Fig.16
Validation of the first natural frequency of the present work with reference [27] in C-F cracked beam at $\frac{c}{h} = 0.3$.
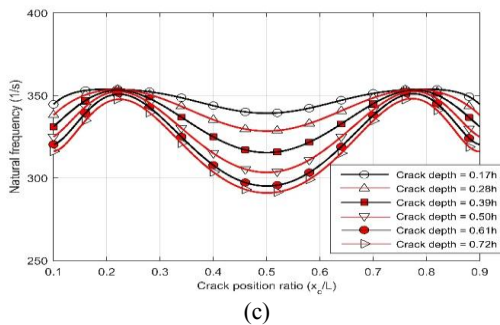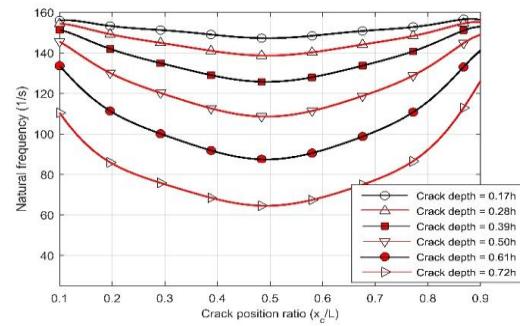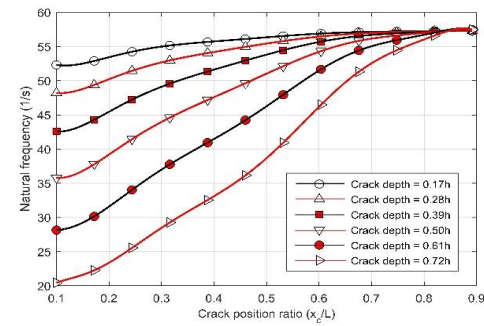

(a)

(b)

(c)

Fig.17
First natural frequency of cracked beam: (a) C-F (b) SS-SS (c) C-C.

Fig. 18 depicts the second natural frequency in terms of different crack positions and depths for three boundary conditions. According to Fig. 18(a) for C-F B.C., the value of natural frequency in all depths is maximized where the crack is located nearly at $x_c/L = 0.2$. Here, the maximum difference between the values of the beam with the deepest crack and the perfect beam is visually detected 2.48%. As the crack positions closer to the free boundary condition, the effect of the crack diminishes on the natural frequency values. By increasing the crack depth, the points corresponding to the minimum natural frequencies take some distance from the middle of the beam.

The second natural frequency for SS-SS B.C. is shown in Fig. 18(b). Here, the value of the natural frequency in each depth is minimized where the crack is located about $x_c/L = 0.88$ or 0.12 and. Also, the maximum value of the natural frequency in the whole crack depths can be achieved where the crack approximately places at the middle of the beam.

Fig. 18(c) demonstrates the influence of the crack on the second natural frequency for C-C B.C. The maximum values of the natural frequency in all depths are estimated where the crack is located at the middle of the beam and near the supports. Also, the values of the natural frequency are minimized where the crack sits at a distance about $L/3$ from the both supports.

By comparing between the first and the second natural frequencies relevant to C-C and SS-SS boundary conditions, it is observed where the value of the first natural frequency is minimized; the value of the second natural frequency is maximized. The greatest change in the first natural frequency of cracked beam in the comparison with the perfect beam is observed in C-F, SS-SS and C-C B.C. almost 64.32%, 59% and 17.8%, respectively, while these changes for the second natural frequency are achieved 60.72%, 50.3% and 17.32% in SS-SS, C-F and C-C B.C., respectively.

3D displays on Figs. 17 and 18 are arranged in Fig. 19 to evaluate the first and the second natural frequencies in terms of different crack depths and positions.
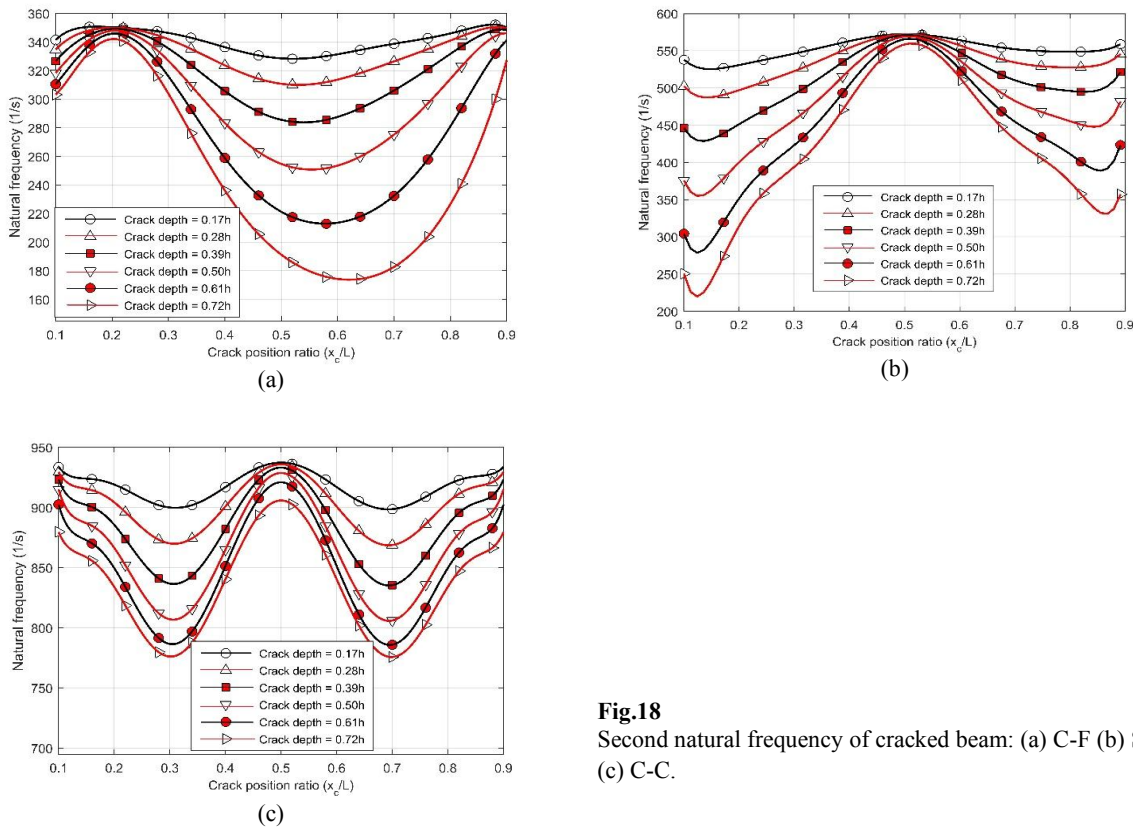

(a)

(b)

(c)

Fig.18
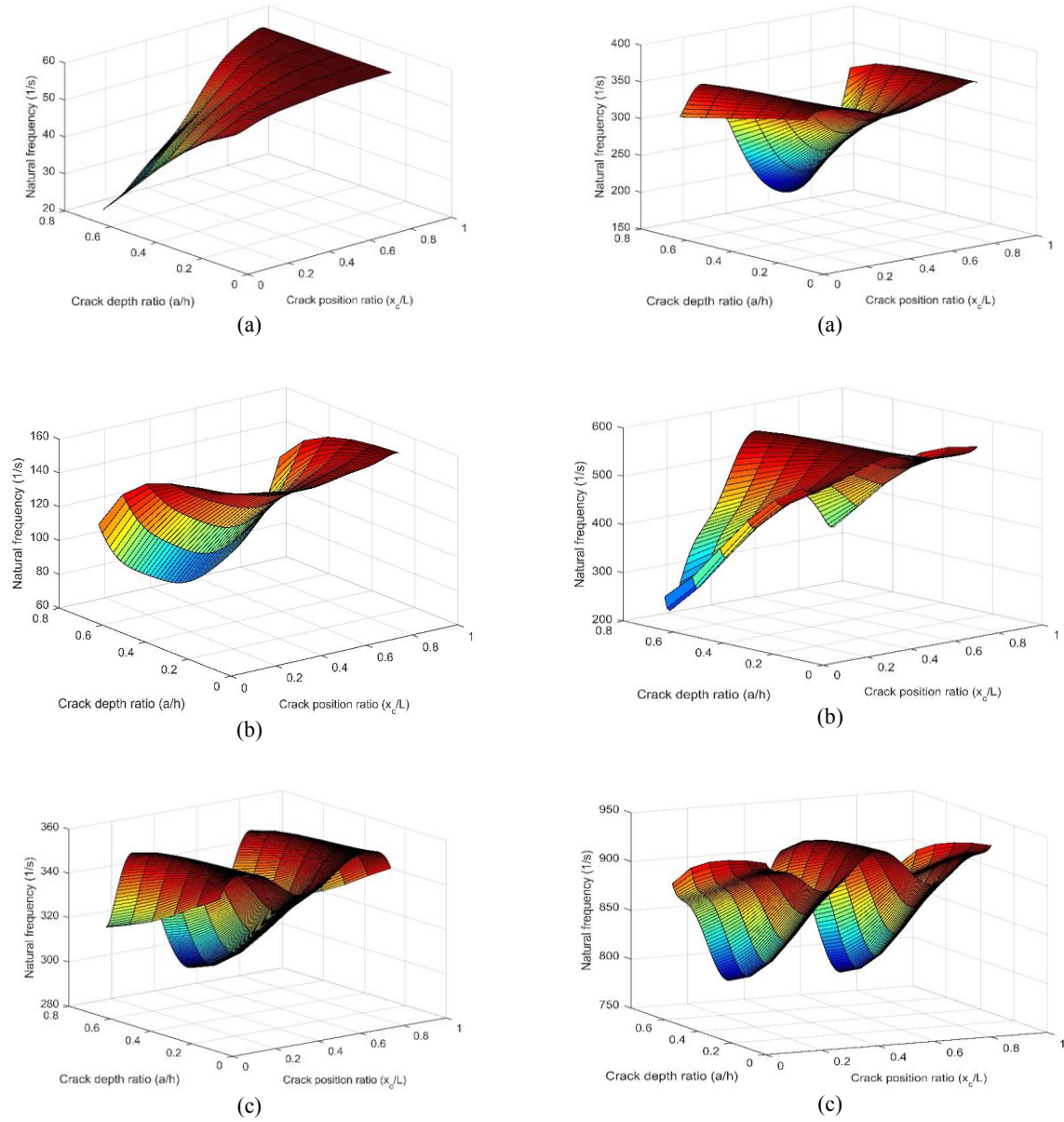Second natural frequency of cracked beam: (a) C-F (b) SS-SS (c) C-C.

Fig.19
Natural frequencies of the cracked beam in terms of crack position and depth: (a) C-F (b) SS-SS (c) C-C.

The first three mode shapes of a cracked beam are demonstrated in Fig. 20 for different boundary conditions as the crack characteristics are identified by $\dfrac{x_c}{L} = 0.4$ and $\dfrac{c}{h} = 0.5$.

In Fig. 20(a), the effect of the crack on the first mode shapes is shown as the opening in elements of near crack for SS-SS B.C. and the sliding in the similar elements for C-C and C-F boundary conditions. A strong likeness can be seen between the results of the first mode shapes in the vibration analysis and the deflection pattern in the statics analysis.

The second mode shapes are illustrated in Fig. 20(b). The influence of the crack on each B.C. is revealed as the sliding in elements of near crack.

Fig. 20(c) shows the third mode shapes in different boundary conditions. The crack makes the opening in near crack elements for SS-SS and C-C and the siding in the similar elements for C-F boundary conditions.

(a)

(b)

(c)
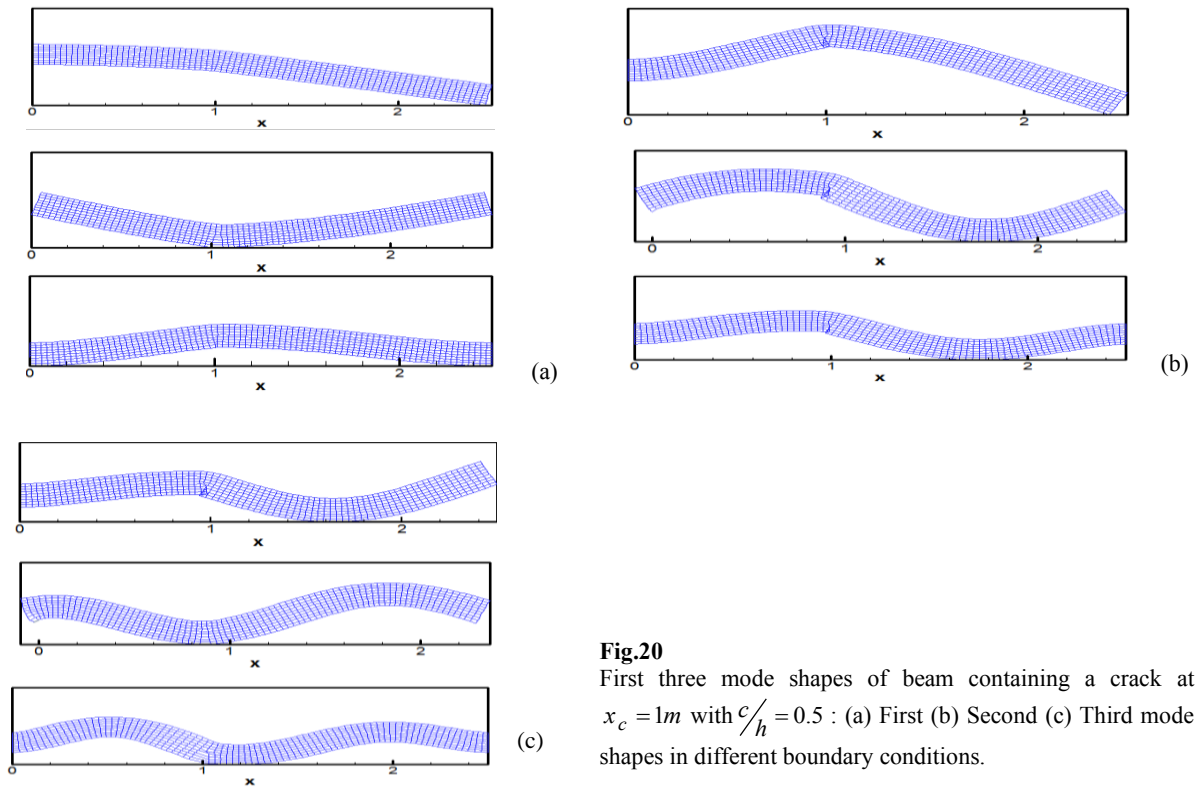
Fig.20
First three mode shapes of beam containing a crack at $x_c = 1m$ with $c/h = 0.5$: (a) First (b) Second (c) Third mode shapes in different boundary conditions.

7   CONCLUSIONS

In this paper, the statics and vibration analyses of two-dimensional cracked isotropic beams were investigated. The XFEM was employed to study the effects of different crack depths and positions on the statics and vibration characteristics. The derivation of XFEM equation for cracked bars and beams was explicitly expressed by developing FEM equations of perfect bars and beams. Two techniques for modifying the numerical integration were applied for diminishing the influence of discontinuity and singularity of the crack zone. One of them was introduced as the increase of the number of Gauss points and the other one was called as the sub-grid technique that its relationships were essentially derived for the perfect and the cracked bars and beams. The results of these two techniques and the normally Gauss integration technique were compared to distinguish their advantages and disadvantages in the analysis of the cracked beam. An eigenvalue equation was developed by extending the stiffness and the mass matrices to determine the natural frequencies and mode shapes. The results of the analysis are reported as follows:
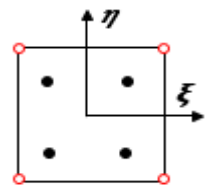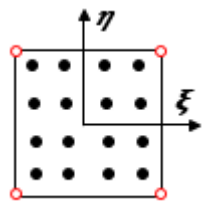
- It is clearly seen that a crack reduces the structure stiffness and the natural frequency.
- A direct proportion between the crack depth and the results of structure deflection can be observed.
- The results show an inverse proportion between the crack depth and the natural frequencies.
- The effects of discontinuity along the crack and the singularity at the crack tip can be reduced by using two techniques for the integration in the enriched and the blended elements.
- The rectangular sub-grid technique is more efficient than the others.
- In determination of the deflection, the SS-SS B.C. possess the most sensitivity to change of the crack depth, while the least sensitivity appears in C-F boundary conditions.
- The crack changes the classical mode shapes in beams.
- If a crack is located near clamped supports, maximum and minimum effects on the deflection can be revealed in C-F and C-C B.C., respectively.

- If a crack is located at the middle of the beam, the influence of the crack on the deflection in SS-SS B.C. will be more than the others. If a crack sits at x_c/L =0.22 or 0.78, the influence of the crack on the first natural frequency for C-C B.C. can be approximately ignored.
- The maximum decrease in the first (second) natural frequency due to crack is seen in C-F, SS-SS and C-C (SS-SS, C-F and C-C) B.C., respectively.

APPENDIX A

$\mathcal{N}^{Gauss}$	ξ_p	w_p	Position of points
2	- 0.5773 + 0.5773	1 1	

APPENDIX B

$\mathcal{N}^{Gauss}$	ξ_p	η_p	w_p	Position of points
4	- 0.5773 0.5773 - 0.5773 0.5773	- 0.5773 - 0.5773 0.5773 0.5773	1 1 1 1	
16	-0.8611 -0.3400 0.3400 0.8611 -0.8611 -0.3400 0.3400 0.8611 -0.8611 -0.3400 0.3400 0.8611 -0.8611 -0.3400 0.3400 0.8611	-0.8611 -0.8611 -0.8611 -0.8611 -0.3400 -0.3400 -0.3400 -0.3400 0.3400 0.3400 0.3400 0.3400 0.8611 0.8611 0.8611 0.8611	0.1210 0.2269 0.2269 0.1210 0.2269 0.4253 0.4253 0.2269 0.2269 0.4253 0.4253 0.2269 0.1210 0.2269 0.2269 0.1210	

APPENDIX C

Nomenclature

a	vector of additional degrees of freedom for modeling crack face	N^{tip}	crack tip shape function matrix
A	area	t	width
b	vector of additional degrees of freedom for modeling crack tip	u	axial displacement
		$u(x)$	displacement field
		$\{u\}$	displacement vector

B	derivative of shape function	$\{u^e\}$	enriched displacement vector
B^{std}	derivative of standard shape function	$\{u^k\}$	sub-grid displacement vector
B^{hev}	derivation of Heaviside shape function	$u^{std}(x)$	standard displacement field
B^{tip}	derivation of crack tip shape function	$u^{enr}(x)$	enriched displacement field
c	crack depth	U	strain energy
C_L	left sub-grid conversion matrix	v	transverse displacement
C_R	right sub-grid conversion matrix	V	Volume
C^{std}	standard conversion matrix	w_p	Gauss weighting factor
C^{hev}	Heaviside conversion matrix	x_c	crack position
C^{tip}	crack tip conversion matrix	x	arbitrary position
D	plane stress stiffness	$\bar{x}$	position of near crack
E	elasticity young modulus	x^*	closest point to $\bar{x}$ on the crack
f^b	crack tip external force vector	x_i	nodal position
f^u	standard external force vector	x_i^k	nodal position of sub-grid
f^a	Heaviside external force vector	x^k	arbitrary position of sub-grid
F	external force vector	$\beta(x)$	crack tip function
h	height	σ	stress vector
$H(x)$	Heaviside function	σ_x	axial stress
I	moment of inertia in the beam	$\delta(x)$	Dirac delta function
J	Jacobian matrix	ε	strain vector
k_L	left sub-grid stiffness matrix	ε_x	axial strain
k_R	right sub-grid stiffness matrix	ε_y	transverse strain
k_{sub}	stiffness matrix for sub-grid	$\varepsilon^{enr}(x)$	enriched strain field
K	stiffness matrix	$\varnothing$	angel of crack coordinate and global coordinate
K_L	improved left sub-grid stiffness matrix	Γ	loaded region
K_R	improved right sub-grid stiffness matrix	γ_{xy}	shear strain
K_{sub}	improved stiffness matrix for sub-grid	$\mathcal{N}^{std}$	set of standard nodal points
L	length	$\mathcal{N}^{hev}$	set of Heaviside nodal points
M	mass matrix	$\mathcal{N}^{tip}$	set of crack tip nodal points
n	the unit outward normal to the crack at x^*	$\mathcal{N}^{Gauss}$	number of integration points within an element
N_i	shape function	$\mathcal{N}^{sub}$	number of sub-grid
N	shape function matrix	ρ	density
N^{std}	standard shape function matrix	t_f	traction force
N^{hev}	Heaviside shape function matrix	ϑ	Poisson ratio
		ω	frequency

REFERENCES

[1] Wriggers P., *2008, Nonlinear Finite Element Methods*, Springer Science & Business Media.

[2]   Reddy J. N., 2014, *An Introduction to Nonlinear Finite Element Analysis: with Applications to Heat Transfer, Fluid Mechanics, and Solid Mechanics*, OUP Oxford.

[3]   Logan D. L., 2011, *A First Course in the Finite Element Method*, Cengage Learning.

[4]   Leissa A. W., Qatu M. S., *2011, Vibrations of Continuous Systems*, McGraw-Hill.

[5]   Rao S. S., Yap F. F., 2011, *Mechanical Vibrations*, Prentice Hall Upper Saddle River.

[6]   Cook R. D., *1994, Finite Element Modeling for Stress Analysis*, Wiley.

[7]   Kahya V., Turan M., 2017, Finite element model for vibration and buckling of functionally graded beams based on the first-order shear deformation theory, *Composites Part B: Engineering* **109**: 108-115.

[8]   Darvizeh M. Darvizeh A., Ansari R., Alijani A., 2015, Pre-and post-buckling analysis of functionally graded beams subjected to statically mechanical and thermal loads, *Scientia Iranica, Transaction B, Mechanical Engineering* **22**: 778-791.

[9]   Alijani A., Darvizeh M., Darvizeh A., Ansari R., 2015, Elasto-plastic pre-and post-buckling analysis of functionally graded beams under mechanical loading, *Proceedings of the Institution of Mechanical Engineers, Journal of Materials Design and Applications* **229**: 146-165.

[10]   Mohammadi S., *2008, Extended Finite Element Method: for Fracture Analysis of Structures*, John Wiley & Sons.

[11]   Khoei A. R., 2014, *Extended Finite Element Method: Theory and Applications*, John Wiley & Sons.

[12]   Biondi B., Caddemi S., 2005, Closed form solutions of Euler–Bernoulli beams with singularities, *International Journal of Solids and Structures* **42**: 3027-3044.

[13]   Nakhaei A., Dardel M., Ghasemi M., Pashaei M., 2014, A simple method for modeling open cracked beam, *International Journal of Engineering-Transactions B: Applications* **28**: 321-329.

[14]   Skrinar M., 2009, Elastic beam finite element with an arbitrary number of transverse cracks, *Finite Elements in Analysis and Design* **45**: 181-189.

[15]   Xiao Y., Huang J., Ouyang Y., 2016, Bending of Timoshenko beam with effect of crack gap based on equivalent spring model, *Applied Mathematics and Mechanics* **37**: 513-528.

[16]   Dolbow J., Belytschko T., 1999, A finite element method for crack growth without remeshing, *International Journal for Numerical Methods in Engineering* **46**: 131-150.

[17]   Moës N., Belytschko T., 2002, Extended finite element method for cohesive crack growth, *Engineering Fracture Mechanics* **69**: 813-833.

[18]   Sukumar N., Moës N., Moran B., Belytschko T., 2000, Extended finite element method for three-dimensional crack modelling, *International Journal for Numerical Methods in Engineering* **48**: 1549-1570.

[19]   Borst R. d., Remmers J. J., Needleman A., Abellan M. A., 2004, Discrete vs smeared crack models for concrete fracture: bridging the gap, *International Journal for Numerical and Analytical Methods in Geomechanics* **28**: 583-607.

[20]   Kang Z., Bui T. Q., Saitoh T., Hirose S., 2017, Quasi-static crack propagation simulation by an enhanced nodal gradient finite element with different enrichments, *Theoretical and Applied Fracture Mechanics* **87**: 61-77.

[21]   Alijani A., Mastan Abadi M., Darvizeh A., Abadi M. K., 2018, Theoretical approaches for bending analysis of founded Euler-Bernoulli cracked beams, *Archive of Applied Mechanics* **88 :**875-895.

[22]   Mottaghian F., Darvizeh A., Alijani A., 2018, A novel finite element model for large deformation analysis of cracked beams using classical and continuum-based approaches*, Archive of Applied Mechanics* **2018**: 1-36.

[23]   Matbuly M., Ragb O., Nassar M., 2009, Natural frequencies of a functionally graded cracked beam using the differential quadrature method, *Applied Mathematics and Computation* **215**: 2307-2316.

[24]   Nahvi H., Jabbari M., 2005, Crack detection in beams using experimental modal data and finite element model, *International Journal of Mechanical Sciences* **47**: 1477-1497.

[25]   Orhan S., 2007, Analysis of free and forced vibration of a cracked cantilever beam, *NDT & E International* **40**: 443-450.

[26]   Attar M., Karrech A., Regenauer-Lieb K., 2014, Free vibration analysis of a cracked shear deformable beam on a two-parameter elastic foundation using a lattice spring model, *Journal of Sound and Vibration* **333**: 2359-2377.

[27]   Behzad M., Ebrahimi A., Meghdari A., 2008, A new continuous model for flexural vibration analysis of a cracked beam, *Polish Maritime Research* **15**: 32-39.

[28]   Shifrin E., Ruotolo R., 1999, Natural frequencies of a beam with an arbitrary number of cracks, *Journal of Sound and Vibration* **222**: 409-423.

[29]   Bachene M., Tiberkak R., Rechak S., 2009, Vibration analysis of cracked plates using the extended finite element method, *Archive of Applied Mechanics* **79**: 249-262.

[30]   Natarajan S., Baiz P. M., Bordas S., Rabczuk T., Kerfriden P., 2011, Natural frequencies of cracked functionally graded material plates by the extended finite element method, *Composite Structures* **93**: 3082-3092.

[31]   Nguyen-Thoi T., Rabczuk T., Lam-Phat T., Ho-Huu V., Phung-Van P., 2014, Free vibration analysis of cracked Mindlin plate using an extended cell-based smoothed discrete shear gap method (XCS-DSG3), *Theoretical and Applied Fracture Mechanics* **72**: 150-163.